Characterization of the $K\beta$ spectral profile for vanadium

L. F. Smale, C. T. Chantler,[*] and M. N. Kinnane

School of Physics, University of Melbourne, Parkville, Victoria 3010, Australia

J. A. Kimpton

Australian Synchrotron, 800 Blackburn Road, Clayton, Victoria 3168, Australia

D. N. Crosby

Department of Physics, University of Oxford, Oxford OX1 3PU, United Kingdom

Characteristic radiation is used extensively in most high-accuracy x-ray experiments as a standard for calibration, both in laboratory physics and in astrophysics. $K\alpha$ and $K\beta$ radiations have complex asymmetric structure in their spectral profiles, especially for transition metals. Instrumental broadening in x-ray experiments shifts peak energies by small but significant amounts, especially for critical investigations. The spectral profiles must include an account of instrumental broadening so as to be able to transfer the calibration between experiments. We present a transferable characterization of the vanadium $K\beta$ spectral profile, using high-accuracy laboratory experiments. The peak energy of vanadium $K\beta_1$ is then found to be 5426.962 ± 0.015 eV. This result decreases the uncertainty by a factor of 4.7 compared with Bearden and Burr [Rev. Mod. Phys. **39**, 125 (1967)]. Characterization of the profile also permits an accurate and transferable standard and methodology. In the Supplemental Material we present the full profile with uncertainties for use in further analysis using the methodology presented.

I. INTRODUCTION

Fluorescent characteristic radiation results from atomic transitions where an electron decay fills a vacancy. The excitation process that creates the vacancy may also excite other electrons leaving other vacancies, yielding a fluorescent decay energy dependent upon the process involved. Thus characteristic radiation is produced by dominant transitions and an array of satellites.

A number of excitation processes produce characteristic radiation, including electron bombardment, x-ray absorption, and inelastic x-ray scattering. These processes all involve an energetic incoming particle exciting the atom. When the incoming particle has an energy just above threshold, the excited states and the shape of the characteristic energy profile sensitively depend upon the energy of the incoming particle [1–3]. However, it has been found that for electron bombardment, when the energy of the electron is at least 2.5 to 3 times the threshold energy of the dominant transition, the excited state and thus the profile shape of the characteristic radiation stabilize and indeed appear to be approximated well by the latest predictions from relativistic quantum mechanics, following the sudden approximation for the excitation process [4]. This condition makes it possible to characterize the profile of $K\beta$ radiation in a way that is robust to incoming electron energy variation.

Authors have argued for standard x-ray sources using a fixed anode tube, for rotating anode sources, for exotic synchrotron x-ray excitation, and for electron-beam ion-trap excitations in order to produce a clean or well-defined spectral profile which can be used as a calibration standard. In this work we use an exotic location but a simple fixed source excitation following the standard technique of many past researchers. The question is, what is the stable profile which is thereby obtained, and how can it be robustly used, fitted, and modeled in secondary and perhaps critical experiments?

The far-from-threshold spectral profile of the characteristic radiation of an element [5] requires advanced relativistic quantum theory for its elucidation. Characteristic radiation has been used for decades in most high-accuracy x-ray experiments as a standard for calibration. Improving the understanding of the spectral profile of characteristic $K\alpha$ and $K\beta$ radiation under these circumstances will improve measurements in the x-ray regime and will provide reliable data from which insights into theory may flow.

Experimentally, spectral profiles for characteristic radiation have been described by semiempirical fitting of 5 or 7 component peaks for the $K\alpha$ spectra [6,7]. Theoretical models of the characteristic radiation profile shape are dominated by diagram lines, representing x-ray emission from atomic transitions with electron decay, from the ground state plus a core vacancy and an excited electron to the ground state with the core vacancy filled and a higher n vacancy. Additional components, theoretically and empirically, are contributed by satellite lines caused by shake-up and shake-off effects. This set of transitions is complex, especially for elements with open subshells such as the transition metals. Progress in such theory has been slow until recently [8,9]. The empirical modeling through fitting functions tends to conceal part of the theoretical complexity by using the sum of a small number of Lorentzian, Gaussian, Voigt, or instrumental functions. Nevertheless, important physical insight is often claimed for these empirical components, which is also worthy of investigation.

A concerted effort to experimentally characterize the experimental energies of characteristic radiation was undertaken and compiled by Bearden and Burr in 1967 [10]. This has been complemented by theoretical computations by Desclaux [11]

---

*Corresponding author: chantler@unimelb.edu.au

TABLE I. Characteristic radiation peak data. The V $K\alpha$ data are from Chantler *et al.* [18]; the rest of the data are from Deslattes *et al.* [12]. The peak energies of the $K\beta$ radiation have an uncertainty larger than those for $K\alpha$ energies by an order of magnitude.

Spectral profile peak	Reference peak energy (eV)	Peak energy uncertainty (ppm)
Titanium $K\alpha_1$	4510.899	2.08
Titanium $K\alpha_2$	4504.920	2.09
Vanadium $K\alpha_1$	4952.131	1.21
Vanadium $K\alpha_2$	4944.651	2.22
Chromium $K\alpha_1$	5414.804	1.31
Chromium $K\alpha_2$	5405.538	1.31
Manganese $K\alpha_1$	5898.801	1.42
Manganese $K\alpha_2$	5887.685	1.43
Vanadium $K\beta_1$	5427.32	13.0

and Deslattes *et al.* [12] based on the relativistic approaches of Grant [13]. Recently, much experimental work has sought good empirical models of the spectral profiles of the radiation [14–16]. Deslattes *et al.* [12] compiled this experimental work in tables of energies of the observed maxima of characteristic spectra. As shown in Table I, uncertainties in peak energies reported for $K\alpha$ for Z from 22 to 26 are of the order of 1 to 2 parts per million (ppm). However, the peak energy of the vanadium $K\beta$ profile [10] has an uncertainty an order of magnitude larger at 13 ppm.

The data collection methods used in this body of research generally used a double-flat-crystal spectrometer with the Bond method [6,7,17] or a curved-crystal spectrometer [14]. Raw spectra are often deconvolved with a measured or fitted instrumental broadening. Either way, each spectrum is fitted empirically. The peak of each empirical fit has normally been used as the measure of each peak energy.

It is not immediately clear how to use these characterizations as standards in experiments with a different instrumental broadening. Chantler *et al.* [18] addressed this concern by providing a consistent set of empirical fit functions for a range of elements with allowances for typical functional instrumental broadening. In particular, a prescription of the influence and effect of specific broadening on the robustness of the measures of transition energy can thereby be investigated and improved.

A large volume of research has targeted $K\beta/K\alpha$ x-ray intensity ratios [19]. Perhaps 40 papers on this are found in *Physical Review*, with hundreds appearing in other journals [20–22]. Most such publications rely upon low-resolution solid-state detectors measuring the gross intensity of the lines, which can neither resolve the detailed shape of the $K\beta$ spectra nor provide high-accuracy energies. Of course, by being particularly low resolution, the value returned from energy calibration will be an effective weighted mean of the profile intensity and a very different energy compared with the medium-resolution peak energy.

Profiles of chemical energy shifts of the V $K\beta$ spectrum of compounds of vanadium compared with that of pure vanadium have also been conducted using more sensitive instruments [23,24]. Those works are focused on changes in peak separation, perhaps with uniform instrumental broadening, and thus do not attempt to report the detailed line shape on an absolute

energy scale. An interesting recent paper on this area [25] discusses the components of $K\beta$ transitions and satellites but not for vanadium, and indeed, there are no absolute energies reported in that paper.

Thus the only report of which we are aware of a measurement of the characteristic V $K\beta$ line on a claimed well-defined energy scale is by Bearden and Burr [10]. That paper reports the peak energy but requires recalibration by Deslattes *et al.* [12]. After recalibration it is provided as 5427.320(71) eV. No information is provided about how instrumental broadening was dealt with. Noting that V $K\beta$ is an asymmetric line, it is likely that this literature value is significantly affected by shifts caused by instrumental broadening. A theoretical calculation of the energy of the peak of V $K\beta$ is 5430.00(94) eV [12]. The 3.4 standard error discrepancy between theory and experiment is unlikely to be explained by statistical fluctuation and points to a problem in either theory or experiment.

This paper presents a measurement of the vanadium $K\beta$ spectral profile produced by electron bombardment far above the threshold energy and a transferable characterization of the profile leading to a measurement of the energy of vanadium $K\beta_1$. The inclusion of broadening effects in the fitting method enables the results to be transferable to a large range of experimental conditions. Specifically, the characterization can be used in a straightforward manner in experiments where the level of instrumental broadening is difficult to determine.

II. EXPERIMENTAL SETUP

The source of the characteristic radiation was a set of transition-metal foils ($Z = 22$ to 26), each of which was placed in a 20-keV electron beam produced by an electron gun. This source produced $K\alpha$ and $K\beta$ radiations with incident energies far above threshold for each of the metal foils. The radiation source was used for calibration lines as well as for the V $K\beta$ profile itself.

Data collection involved using a Johann geometry curved-crystal spectrometer with position-sensitive x-ray detection. Figure 1 shows a diagram of the setup in terms of the
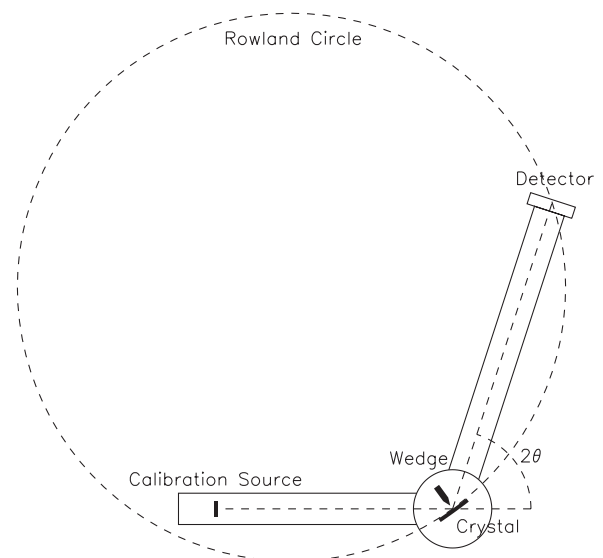

FIG. 1. Schematic diagram of the experimental setup.

three major experimental variables involved: the chosen transition-metal target that emits the characteristic radiation (the calibration source), the angle of the arm that the detector sits on (2θ), and an adjustable "Seemann wedge" to adjust bandpass, instrumental broadening, and the contribution of complex systematics. The angle θ was measured by a gravity-referenced clinometer mounted on the crystal housing. A fixed anode x-ray source at the Oxford energy beam and ion trap (EBIT) [26] was employed.

III. DATA COLLECTION

Seven calibration series were conducted. Each series used a different wedge position and different integration times, so that the diffraction theoretical modeling must make accurate independent predictions of each geometry of each position. Each series was a series of different offset positions of the detector, hence allowing the consistency of the functional with different diffraction angles and geometry to be investigated. The data were collected in pseudoevent mode, so each x-ray event was independently recorded. Within each calibration series, $K\alpha$ and $K\beta$ spectral profiles from $Z = 22$ to 26 were collected. Each spectral profile type was collected at three to five arm angles to sample profiles at different positions on the detector in order to investigate the dispersion function and the detector response function. The remarkable consistency of the results demonstrates the robustness of the code and calibration methodology discussed below. The remaining variance is thus an explicit characterization of all such systematic deficiencies.

IV. $K\alpha$ CALIBRATION PROFILE MODELING

Each $K\alpha$ profile was fitted with functions provided by [18]. Each function of energy or detector position is a sum of six Voigt profiles, with a common Gaussian width to model the instrumental broadening. They map x-ray intensity to x-ray energy. Five fitting parameters were used in the fits of each detector profile: (i) an energy offset, (ii) an energy scale (in eV/mm) to map from detector position to energy, (iii) an intensity scale, (iv) a constant intensity background, and (v) a common Gaussian broadening width representing the additional instrumental broadening of the spectrometer system.

These highly accurate $K\alpha$ characterizations allow the assignment of peak energies to the peak detector positions for each spectrum at each clinometer voltage. Figure 2 illustrates how one such fit leads to two calibration points. The residuals show a small structure which is well centered on the main component peaks and contains noise within one standard deviation.

V. VANADIUM $K\beta$ PROFILE MODELING

As well as the standard reference calibration profiles, V $K\beta$ profiles were also collected and characterized on intensity and detector position axes. To define a characteristic line shape function, each of the spectra were fit with a sum of three Voigt functions with a common Gaussian width σ and a constant intensity background B. The ith Voigt function used in the
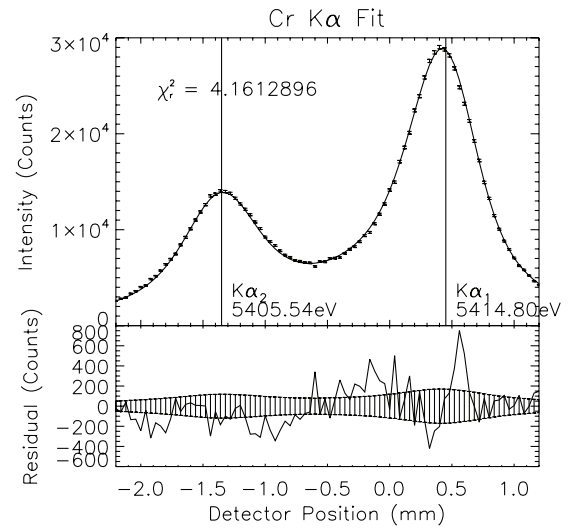

FIG. 2. Typical fit of Cr $K\alpha$ spectrum, yielding two calibration points (Cr $K\alpha_1$ and Cr $K\alpha_2$, constraining the spectrometer dispersion (calibration) function. The fit has a χ_r^2 of 4.2. The $K\alpha_1$ peak has an energy of 5414.8045(71) eV and a detector position of 0.4510(12) mm. The $K\alpha_2$ peak has an energy of 5405.5384(71) eV and a detector position of $-1.3507(21)$ mm. The crystal clinometer voltage was $-1.705582(11)$ V.

characterization is defined to be

$$
\begin{aligned}
&V(x; A_i, C_i, W_i, \sigma_i) \\
&= A_i \int_{-\infty}^{\infty} \frac{e^{-x'^2/(2\sigma_i^2)}}{\sigma_i \sqrt{2\pi}} \frac{W_i/2}{\pi[(x - C_i - x')^2 + (W_i/2)^2]} \, dx',
\end{aligned}
\tag{1}
$$

where A_i is the integrated area of the Lorentzian profile, C_i is the centroid of the profile, W_i is the Lorentzian full width at half maximum (FWHM), and σ_i is the Gaussian broadening standard deviation. The Gaussian broadening FWHM is $2\sqrt{2\ln 2}\sigma_i \approx 2.35\sigma_i$. Thus the spectra containing a V $K\beta$ spectral profile was modeled with

$$
\begin{aligned}
&P(E; B, \sigma, A_1, C_1, W_1, A_2, C_2, W_2, A_3, C_3, W_3) \\
&= B + \sum_{i=1}^{3} V(E; A_i, C_i, W_i, \sigma).
\end{aligned}
\tag{2}
$$

All the samples of the V $K\beta$ profile were independently measured and fitted with this method. The relative intensities, positions, and widths of the Voigt functions of the fits were consistent with one another. That is, the determined parametrization from one representative profile was found to be within the uncertainty of other profiles and their independent parametrizations. Further, each representative determination was able to be used as a calibration functional for the other profiles. Hence minimum uncertainty results are reported. The characteristic parameters of these fits are shown in Table II, with positions converted to energies. Figure 3 shows a typical fit for one of the vanadium $K\beta$ spectra.

All V $K\beta$ profiles were then refit under the constraints of these optimized parameters. Each refit had free parameters characterizing the overall intensity, position, detector position to energy-scale conversion, instrumental broadening, and the

TABLE II. The full characterization of the V $K\beta$ spectral profile on an absolute energy scale. The parameters are used in Eq. (2). Amplitudes A_i, centroids C_i, and widths W_i of individual components were obtained from a fit on the intensity versus detector position axis. The detector position axis was transformed to an absolute energy scale via the calibration procedure. The Gaussian width σ was 0.804(25) eV. The background was 749(24) counts.

Proportion of area $\frac{A_i}{\sum_{i=1}^{4} A_i}$	Integrated area A_i (counts)	Centroid C_i (eV)	Width W_i (eV)
0.258(21)	160280(12941)	5418.20(35)	18.86(83)
0.236(18)	146750(11207)	5424.50(11)	5.48(21)
0.507(14)	315345(8472)	5426.998(13)	2.498(69)

background of the spectral profile in the specific geometry of the measurement. As each refit had a slightly different instrumental broadening due to geometry changes, the transferable reference position of the peak of each profile was the position of the maximum of the fit function with the Gaussian width set to zero. All refits were reliable and consistent with the original fits as discussed above. Therefore, this characterization allows for a consistent transferable standard in this measurement, in the calibration of the dispersion function, and for any subsequent independent measurement. It enabled a consistent measurement of peak position on any V $K\beta$ profile for any local instrumental broadening.

VI. DISPERSION FUNCTION AND ENERGY CALIBRATION

A dispersion function is required to map a clinometer voltage and a spectral profile measured on a detector position axis (such as in Fig. 3) to a spectral profile measured on an absolute energy axis. The dispersion function consists of a theoretical model of the experimental setup provided by the dynamical diffraction code MOSPLATE [27,28], a clinometer
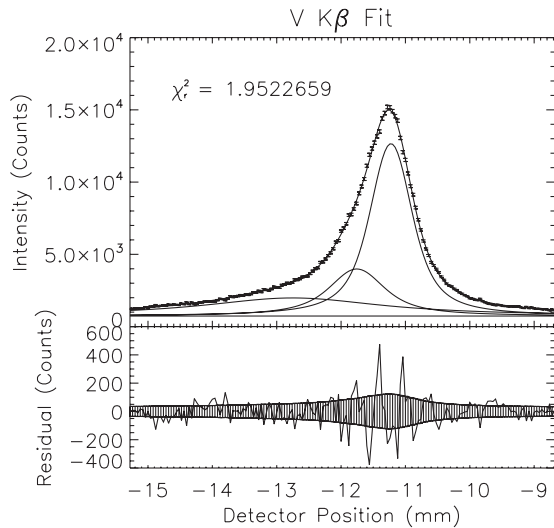
FIG. 3. Typical fit of a V $K\beta$ spectrum. The crystal clinometer voltage was $-1.781742(11)$ V, and the detector position was $-11.234(1)$ mm. The $K\beta_1$ peak has an energy of 5427.104(61) eV.

calibration function, and a detector dispersion calibration function.

MOSPLATE calculates the diffraction profile at the detector (and thus peak position) of a particular energy of an x ray at a particular angle θ. These calculations of peak position sample the MOSPLATE model function for the diffraction profile peak position D as a function of peak energy E (the energy of the x ray) and crystal angle θ:

$$D = D_{\text{mos}}(E,\theta). \quad (3)$$

This model also implicitly defines functions that calculate E and θ from the remaining variables:

$$E = E_{\text{mos}}(D,\theta), \quad (4)$$

$$\theta = \theta_{\text{mos}}(D,E). \quad (5)$$

The clinometer calibration function $I(V;P_I)$ maps the clinometer voltage V to the dispersion crystal angle θ:

$$\theta = -I(V;P_I), \quad (6)$$

where $I(V;P_I)$ is defined to be

$$I(V;P_I) = \text{asin}\left(\frac{V - P_{I,2}}{P_{I,0}}\right) - P_{I,1} + \sum_{i=0}^{n} P_{I,(i+3)}(V - P_{I,2})^i \quad (7)$$

and P_I is the vector of fitting parameters.

The second calibration function, the detector dispersion calibration function $D(x;P_D)$, maps the recorded detector position x in output units to the theoretical detector position D in millimeters. The map from x to D was defined by

$$D(x;P_D) = \sum_{i=0}^{1} P_{D,i} x^i, \quad (8)$$

where P_D is the vector of fitting parameters.

Using this dispersion function, an energy can be assigned to a detector position x for any clinometer voltage V through

$$E(x,V;P_D,P_I) = E_{\text{mos}}(D(x;P_D), -I(V;P_I)). \quad (9)$$

Equations (7) and (8) define the calibration of an experimental configuration (i.e., a calibration series). The calibration process was reduced to simultaneously finding the P_I and P_D fitting parameters that best fit the $K\alpha$ data and produced an internally consistent measurement of the V $K\beta$ peak energy for each calibration series. This process makes optimum use of the statistical information for the determination of the profile and dispersion function.

VII. DISPERSION AND DETECTOR

The process to find the fitting parameters P_I and P_D for the calibration entails four major steps: clinometer precalibration, clinometer calibration first estimate, calibration fitting, and detector scale correction. First, the clinometer precalibration made a preliminary characterization of the angle of incline to voltage function $V_{\text{pre}}(I)$ of the clinometers:

$$V_{\text{pre}}(I) = P_{V,0} \sin(I - P_{V,1}) - P_{V,2} + \sum_{i=0}^{8} P_{V,(i+3)} V^i. \quad (10)$$
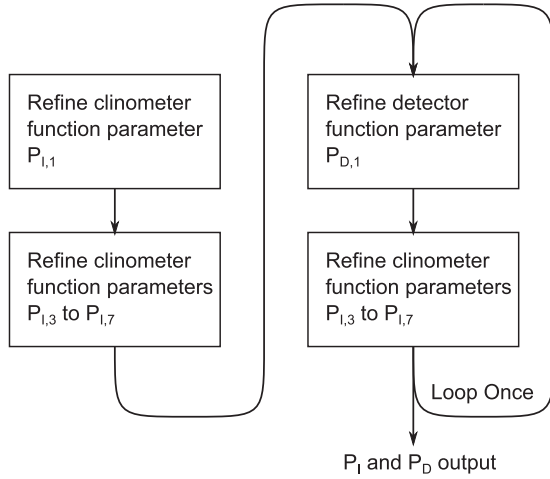
FIG. 4. Schematic of the calibration fitting stages. Each stage is a round of refitting.

Second, an estimate of the clinometer calibration function involved generating data with the $V_{pre}(I)$ function, inverting the data, then fitting the inverted data with $I(V; P_I)$ [Eq. (7)], where n (the order of the polynomial involved) was set to 3. This function includes parameters for the clinometer response and also for typical mechanical response functions. The fitted P_I parameters then provided a reasonable estimate as to how the clinometers have functioned in the setup.

Finally, calibration fitting was a six-stage process that started with estimates of P_I and P_D (Fig. 4). Each stage made a refinement of either P_I or P_D through one round of refitting.

The six-stage calibration fitting used the interlinked K_α peak energy, peak position, and clinometer voltage calibration data. These data were processed in one of two ways prior to fitting to generate the dispersion function. Either I_{data} or D_{data} was calculated. I_{data} is a set of calculated data that corresponds to the expected clinometer angle for each peak based on the energy and detector position.

$$I_{data} = -\theta_{mos}(D(x, P_D), E). \quad (11)$$

It has uncertainty ΔI_{data}:

$$\Delta I_{data}^2 = \left(\frac{\partial \theta_{mos}}{\partial E} \Delta E\right)^2 + \left(\frac{\partial \theta_{mos}}{\partial D}\right)^2$$
$$\times \left[\sum_{ij} \frac{\partial D}{\partial P_{D,i}} \frac{\partial D}{\partial P_{D,j}} C_{D,ij} + \left(\frac{\partial D}{\partial x} \Delta x\right)^2\right]. \quad (12)$$

D_{data} is a set of calculated data that corresponds to the expected theoretical detector position for each peak based on the energy and crystal angle.

$$D_{data} = D_{mos}(E, -I(V; P_I)). \quad (13)$$

It has uncertainty ΔD_{data}:

$$\Delta D_{data}^2 = \left(\frac{\partial D_{mos}}{\partial E} \Delta E\right)^2 + \left(\frac{\partial D_{mos}}{\partial \theta}\right)^2$$
$$\times \left[\sum_{ij} \frac{\partial I}{\partial P_{I,i}} \frac{\partial I}{\partial P_{I,j}} C_{I,ij} + \left(\frac{\partial I}{\partial V} \Delta V\right)^2\right]. \quad (14)$$

The six stages of fitting were designed to find a set of fitting parameters P_I and P_D that are self-consistent. Each fit used one of two sets of axes: axis set 1, which was I_{data} vs V, and axis set 2, which was D_{data} vs x. The first fit was of axis set 1 (calculated using the estimated P_D parameters) with $I(V; P_I)$ only allowing the refinement of $P_{I,1}$. This found an overall offset to $I(V; P_I)$. The second fit was again of axis set 1 with $I(V; P_I)$ using the P_I from fit 1 as an estimate, this time only allowing the refinement of $P_{I,3}$ through $P_{I,7}$. This fitted the fine details of $I(V; P_I)$. The third fit was of axis set 2 (calculated using the refined P_I parameters from the second fit) with $D(x; P_D)$. The fourth fit was of axis set 1 (calculated using the refined P_D parameters from the third fit) with $I(V; P_I)$ only allowing the refinement of $P_{I,3}$ through $P_{I,7}$ (as in the second fit). Fits five and six are a repeat of the third and fourth fits using the output of fit four as the input of fit five. This method generates the P_I and P_D parameters along with associated covariance error matrices C_I (from the sixth fit) and C_D (from the fifth fit). These six stages of this third step are diagramed in Fig. 4.

Finally, a detector scale refinement investigated the value of $P_{D,1}$ (the detector scale) by grid search to minimize the uncertainty and variance of the weighted mean of the peak energy of all V $K\beta$ spectra. A low uncertainty (variance) in the weighted mean represents greater consistency between independent spectra. For each $P_{D,1}$ value in the grid search there was a three-step process: (1) a fit of axis set 1 to refine the clinometer calibration function in the context of that detector scale, (2) modeling of the V $K\beta$ peak position and clinometer voltage data for all of the calibration series using Eq. (9) to generate a set of V $K\beta$ peak energies and uncertainties for the calibration series, and (3) computing the weighted mean and corresponding uncertainty from the variance of the set of energies. The final calibration was then represented by the refined fitting parameters, which reflect the experimental minimization of systematic variance around V $K\beta$.

VIII. ENERGY UNCERTAINTIES

The uncertainty in the energy of a peak position ΔE is made up of four sources of uncertainty: (i) the statistical precision of the determination of the peak of the spectral fit (Δx_{fit}), (ii) the uncertainty due to the detector dispersion fit, (iii) the noise in clinometer voltage ΔV, and (iv) the clinometer calibration function fitting uncertainties. The following equation for ΔE is a sum of the four terms representing these uncertainty components:

$$\Delta E^2 = \left(\frac{\partial E}{\partial x} \Delta x_{fit}\right)^2 + \sum_{ij} \frac{\partial E}{\partial P_{D,i}} \frac{\partial E}{\partial P_{D,j}} C_{D,ij}$$
$$+ \left(\frac{\partial E}{\partial V} \Delta V\right)^2 + \sum_{ij} \frac{\partial E}{\partial P_{I,i}} \frac{\partial E}{\partial P_{I,j}} C_{I,ij}. \quad (15)$$

$C_{D,ij}$ is the i, jth element of the covariance error matrix from the detector dispersion function fit, while $C_{I,ij}$ is the i, jth element of the covariance error matrix from the clinometer calibration function fit. Table III shows average values of these various contributions to ΔE for a single V $K\beta$ spectrum.

TABLE III. Error budget for the peak energy of the three spectral profiles of V $K\beta$ that go into the final energy determination. Since the three determined energies are consistent, the final energy measurement has a smaller uncertainty. The value of $\sqrt{(\chi_r^2)}$ for the clinometer calibration fit was 8.3, while its value for the detector dispersion function fit was 18.6.

Uncertainty source	Average contribution to energy uncertainty for an individual V $K\beta$ spectrum (ppm)
V $K\beta$ spectrum fit $\frac{\partial E}{\partial x}\Delta x_{\text{fit}}$	0.98
Detector dispersion function fit $\sqrt{\sum_{ij}\frac{\partial E}{\partial P_{D,i}}\frac{\partial E}{\partial P_{D,j}}C_{D,ij}}$	0.021
Clinometer noise $\frac{\partial E}{\partial V}\Delta V$	1.3
Clinometer calibration fit $\sqrt{\sum_{ij}\frac{\partial E}{\partial P_{I,i}}\frac{\partial E}{\partial P_{I,j}}C_{I,ij}}$	0.12
Total uncertainty	1.6

IX. $K\beta$ PEAK ENERGY

Fits of the V $K\beta$ spectra provide relatively independent measurements of the peak energy of V $K\beta$. These peak energies are shown in Fig. 5. There is a systematic functional in the dispersion of measured energies with the crystal angle. These data are pooled with their weighted mean, reflecting the total uncertainty including the remnant systematic error.

Combining these data using a weighted mean results in a measurement of the V $K\beta$ profile peak energy of 5426.962(15) eV (2.7 ppm uncertainty). This measurement is inconsistent with the theoretical value of 5430.00(94) eV [12]. The 3.038-eV discrepancy is just over 3.2 standard deviations and is reflective of the theoretical inaccuracy and imprecision.

The uncertainty of this measurement is a factor of 4.7 improvement over the experimental literature value of 5427.320(71) eV (13 ppm uncertainty) [10]. The 0.358 eV
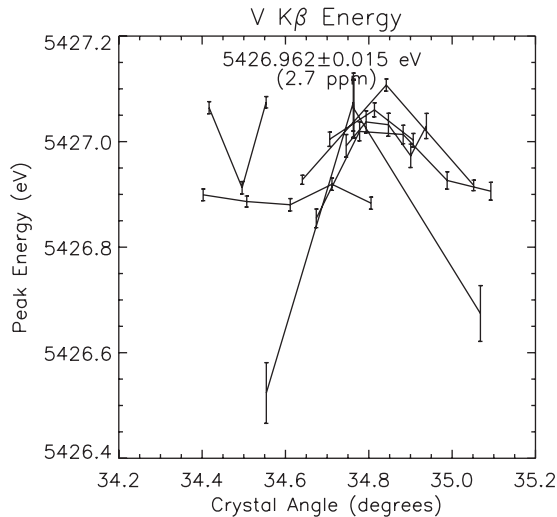

FIG. 5. The peak energies of the fits of individual V $K\beta$ energy spectra. Each of the seven series represents a subset of the data corresponding to a different configuration of the spectrometer. Hence each series must be modeled with a different prediction of the dynamical diffraction code suited to the geometry. Within each subset consecutive points correspond to a methodical stepping of arm position (θ) so that each profile falls on a different part of the detector area. The variance observed is a sign of limitations and systematics of the whole procedure. Therefore the pooled variance correctly represents the robustness of the final determination of profile and energy.

discrepancy is just over 5.0 standard deviations of the previous work. This discrepancy is therefore unlikely to be the result of a statistical fluctuation but is likely evidence of error in one of the two experimental values, possibly due to the inconsistency of instrumental broadening in the prior work or a discrepancy in the characterization of the shape (and thus the peak energy) of the spectrum. Since an account of instrumental broadening is not provided for in the prior work, the discrepancy may be attributable to instrumental broadening therein.

X. USE OF THE CHARACTERIZATION OF VANADIUM $K\beta$

We have presented a transferable characterization of V $K\beta$ in terms of a sum of Voigt functions with a common instrumental (Gaussian) broadening (Table II). For an arbitrary experiment, the instrumental broadening should be refitted to the relevant profile, while the relevant contributions and widths of each component should remain the same. Fitting of an overall amplitude, the energy scale, and the background to the experimental data should be all that is required to maintain the accuracy of the transfer.

Specifically, we measure the V $K\beta$ profile and fit it with

$$P_{\text{fit}}(X;B,\sigma,A,X_1,X_2)$$
$$= P\left(X;B,\sigma,A,X_1,W_1\frac{X_2-X_1}{C_2-C_1},AA_2/A_1,X_2,W_2\frac{X_2-X_1}{C_2-C_1},\right.$$
$$\left. AA_3/A_1,(C_3-C_1)\frac{X_2-X_1}{C_2-C_1}+X_1,W_3\frac{X_2-X_1}{C_2-C_1}\right), \quad (16)$$

where the A_i, C_i, and W_i come from Table II and the X_i parameters are the positions of the first two Voigt peaks, A is the area of the first peak, σ is the Gaussian width of all the Voigt peaks, and B is the background height. This characterization of V $K\beta$ can be usefully transferred to other experiments to generate calibration points for high-accuracy x-ray experiments. The absolute value of the determined peak free from instrumental broadening should then correspond to our result with the given uncertainty. In the Supplemental Material [29] we present the full profile with uncertainties for use in further analysis using the methodology presented.

XI. CONCLUSION

The spectral profile of V $K\beta$ was measured and characterized in a transferable way. The characterization involved

modeling the profile with four Lorentzian peaks convolved with an overall Gaussian. The Gaussian is recommended as a reasonable approximation for modeling additional instrumental broadening. The individual widths, positions, and relative intensities for each Lorentzian component are described and tabulated. The V $K\beta$ peak energy was found to be 5426.962(15) eV. This is an improvement in uncertainty by a factor of 4.7 over prior work. Further, the full profile is deposited for general use or to directly compare to a calibration profile without the parametric modeling. We recommend that the component modeling is reliable and much more accurate than previous approaches and is a recommended standard methodology for future x-ray calibration.

ACKNOWLEDGMENT

[1] S. Galambosi, H. Sutinen, A. Mattila, K. Hämäläinen, R. Sharon, C. C. Kao, and M. Deutsch, Phys. Rev. A **67**, 022510 (2003).

[2] M. Fritsch, C. C. Kao, K. Hämäläinen, O. Gang, E. Förster, and M. Deutsch, Phys. Rev. A **57**, 1686 (1998).

[3] M. Deutsch, O. Gang, K. Hämäläinen, and C. C. Kao, Phys. Rev. Lett. **76**, 2424 (1996).

[4] C. T. Chantler, J. A. Lowe, and I. P. Grant, J. Phys. B **46**, 015002 (2012).

[5] C. T. Chantler, J. A. Lowe, and I. P. Grant, Phys. Rev. A **82**, 052505 (2010).

[6] M. Deutsch, G. Hölzer, J. Härtwig, J. Wolf, M. Fritsch, and E. Förster, Phys. Rev. A **51**, 283 (1995).

[7] G. Hölzer, M. Fritsch, M. Deutsch, J. Härtwig, and E. Förster, Phys. Rev. A **56**, 4554 (1997).

[8] C. T. Chantler, A. C. L. Hayward, and I. P. Grant, Phys. Rev. Lett. **103**, 123002 (2009).

[9] J. A. Lowe, C. T. Chantler, and I. P. Grant, Phys. Lett. A **374**, 4756 (2010).

[10] J. A. Bearden and A. F. Burr, Rev. Mod. Phys. **39**, 125 (1967).

[11] J. P. Desclaux, At. Data Nucl. Data Tables **12**, 312 (1973).

[12] R. D. Deslattes, E. G. Kessler, P. Indelicato, L. de Billy, E. Lindroth, and J. Anton, Rev. Mod. Phys. **75**, 35 (2003).

[13] I. P. Grant, Adv. Phys. **19**, 747 (1970).

[14] D. F. Anagnostopoulos, R. Sharon, D. Gotta, and M. Deutsch, Phys. Rev. A **60**, 2018 (1999).

[15] D. F. Anagnostopoulos, D. Gotta, P. Indelicato, and L. M. Simons, Phys. Rev. Lett. **91**, 240801 (2003).

[16] J. Schweppe, R. D. Deslattes, T. Mooney, and C. J. Powell, J. Electron Spectrosc. Relat. Phenom. **67**, 463 (1994).

[17] W. L. Bond, Acta Crystallogr. **13**, 814 (1960).

[18] C. T. Chantler, M. N. Kinnane, C.-H. Su, and J. A. Kimpton, Phys. Rev. A **73**, 012508 (2006).

[19] S. Raj, H. C. Padhi, P. Palit, D. K. Basa, M. Polasik, and F. Pawłowski, Phys. Rev. B **65**, 193105 (2002).

[20] O. Sogut, E. Bykkasap, and H. Erdogan, Radiat. Phys. Chem. **64**, 343 (2002).

[21] S. Raj, H. C. Padhi, D. K. Basa, M. Polasik, and F. Pawowski, Nucl. Instrum. Methods Phys. Res., Sect. B **152**, 417 (1999).

[22] H. C. Padhi, C. R. Bhuinya, and B. B. Dhal, J. Phys. B **26**, 4465 (1993).

[23] S. Fazinic, M. Jaksic, L. Mandic, and J. Dobrinic, Phys. Rev. A **74**, 062501 (2006).

[24] L. Mandić, S. Fazinić, and M. Jakšić, Phys. Rev. A **80**, 042519 (2009).

[25] S. P. Limandri, A. C. Carreras, R. D. Bonetto, and J. C. Trincavelli, Phys. Rev. A **81**, 012504 (2010).

[26] J. D. Silver, A. J. Varney, H. S. Margolis, P. E. G. Baird, I. P. Grant, P. D. Groves, W. A. Hallett, A. T. Handford, P. J. Hirst, A. R. Holmes *et al.*, Rev. Sci. Instrum. **65**, 1072 (1994).

[27] C. T. Chantler, J. Appl. Crystallogr. **25**, 674 (1992).

[28] C. T. Chantler, J. Appl. Crystallogr. **25**, 694 (1992).

[29] See Supplemental Material at http://link.aps.org/supplemental/10.1103/PhysRevA.87.022512 for further analysis.